J Sol-Gel Sci Technol (2016) 78:159–165
DOI 10.1007/s10971-015-3911-1

ORIGINAL PAPER: SOL-GEL AND HYBRID MATERIALS FOR DIELECTRIC, ELECTRONIC, MAGNETIC AND FERROELECTRIC APPLICATIONS

Magnetocaloric response of submicron (LaAg)MnO_3 manganite obtained by Pechini method

M. E. Amano[1] · I. Betancourt[2] · M. J. Arellano-Jimenez[2] · J. L. Sánchez-Llamazares[3] · C. F. Sánchez-Valdés[3]

Received: 24 August 2015 / Accepted: 2 November 2015 / Published online: 24 November 2015

Abstract Lanthanum-based manganites containing monovalent silver cations and having grain sizes below 0.30 microns were synthesized via Pechini method, by using a moderate calcination temperature (900 °C). The incorporation of Ag^{+} ions into the perovskite crystal structure was verified by means of EDS, EELS, and XPS techniques. Monovalent cations provoked a rhombohedral deformation of the crystal structure, together with the formation of Mn^{3+}–Mn^{4+} pairs yielding to a noticeable ferromagnetic behavior characterized by high saturation magnetization (47 Am^2/kg) and a steep Curie transition at 308 K. This combination of magnetic properties enable an excellent magnetocaloric performance, with magnetic entropy variations of up to 5.6 J/kg K (for magnetic field $\Delta H = 5.0$ T) and refrigerant capacities of up to 184 J/kg.

Graphical Abstract

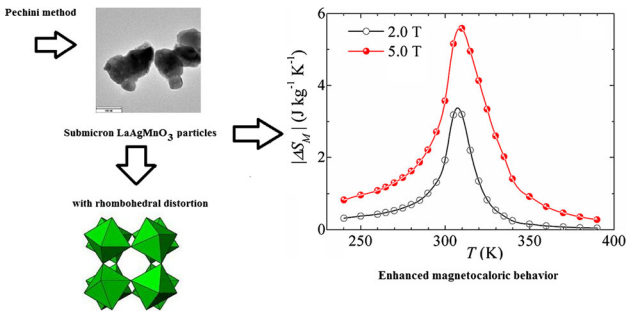

Keywords Mixed valence manganites · Pechini method · Magnetocaloric effect · Magnetic oxides

1 Introduction

The magnetocaloric effect (MCE) refers to the adiabatic temperature change in a material subject to the effect of an external magnetic field. This effect has been extensively studied in La-based manganites with perovskite structure because of the distinctive advantages of these materials: high thermal stability, competitive cost of production and the possibility for modulating their Curie temperatures and spontaneous magnetization over an ample range of temperatures [1–4]. In particular, $LaMnO_3$-based manganites with partial substitution of La^{3+} by divalent cations have shown a strong correlation between electronic properties and the valence and the ionic radius of the doping atoms [2, 3]. For instance, for $La_{1-x}Sr_xMnO_3$ systems, the mixed valence Mn^{3+}–Mn^{4+} pairs (provoked by the divalent Sr^{2+} inclusion) induce mobile holes in the e_g band near the Fermi energy, affecting the conduction and the

I. Betancourt is at sabbatical leave from Instituto de Investigaciones en Materiales, Universidad Nacional Autónoma de México, México D.F. 04510, México.

✉ I. Betancourt
israelb@iim.unam.mx; israelb@unam.mx

[1] Departamento de Materiales Metálicos y Cerámicos, Instituto de Investigaciones en Materiales, Universidad Nacional Autónoma de México, 04510 México, D.F., Mexico

[2] Department of Physics and Astronomy, University of Texas at San Antonio, One UTSA Circle, San Antonio, TX 78249, USA

[3] Instituto Potosino de Investigación Científica y Tecnológica, Camino a la Presa San José 2055, Col. Lomas 4ª, 78216 San Luis Potosí, S.L.P., Mexico

superexchange mechanism (responsible of the antiferromagnetic coupling in manganites) in favor of the double-exchange interaction (DE). This type of interaction promotes ferromagnetic coupling yielding high saturation magnetization values together with high Curie temperatures [5–7]. Partial substitution of La^{3+} by monovalent cations such as K^+, Na^+, and Ag^+ can also promote DE interaction between Mn^{3+}–Mn^{4+} pairs, and hence, a desirable modulation of magnetic properties and consequently of the MCE [8–10]. Previous reports on $La_{1-x}Ag_xMnO_3$ manganites describe in general moderate-to-low magnetic properties, including saturation magnetization below 30 Am^2/kg for silver content $x \leq 0.20$ and variable Curie transition (below room temperature) depending on the synthetic route used [2, 11–15].

An effective way to produce submicron, chemically homogeneous manganites, is the "Pechini method," a soft chemistry process where the formation of an oxide network occurs through the thermal decomposition in air of an amorphous solid, a xerogel [16]. This method allows the formation of small particles with narrow size distribution, together with high chemical homogeneity [17, 18]. In this work, we present and discuss the influence of monovalent Ag^+ cations on the structure, magnetic properties, and MCE performance of submicron $(LaAg)MnO_3$ manganites obtained by Pechini method.

2 Synthesis and methods

Manganite with composition $La_{0.80}Ag_{0.20}MnO_3$ was prepared by the Pechini method with the following precursors: $La(NO_3)_3{\cdot}6H_2O$ (Fluka ≥99.0 %), $AgNO_3$ (J.T. Baker ≥99.7 %), $Mn(NO_3)_2{\cdot}4H_2O$ (Aldrich ≥98.0 %), $C_6H_8O_7$ (Sigma-Aldrich ≥99.8 %), $C_2H_6O_2$ (Sigma-Aldrich, ≥99.8 %), and NH_4OH (Sigma-Aldrich 28.0–30.0 %, 0.99 g/cm^3 density). The initial solution was prepared by dissolving $La(NO_3)_3$ and $Mn(NO_3)_2$ in 100 mL of distilled water with the following concentrations: 0.102 and 0.127 mol/L, respectively. A second dissolution of $AgNO_3$ within 20 mL of distilled water was prepared apart (concentration of 0.121 mol/L), to which 1 mL of NH_4OH was added in order to obtain the soluble diamine–silver complex Ag $[(NH_3)_2]^+$ according to the following reaction:

$$Ag^+_{(ac)} + 2\ NH_4OH_{(l)} \leftrightarrow\ Ag\ \left[(NH_3)_2\right]^+_{(ac)} + H_2O_{(l)}$$

This step aims to change the redox potential of the Ag^+ cations, which reacts spontaneously with Mn^{2+} cations to form insoluble metallic Mn and Ag^{2+}. A remanent unreacted portion of $AgNO_3$ acts as basifier agent. A third, separated mixture of citric acid and ethylene glycol was prepared by the following two-step process: (a) dissolution of $C_6H_8O_7$ within 30 mL of distilled water with the molar ratio of metallic cations/citric acid of 1:2 in order to ensure a complete chelation of metallic cations (b) slow addition of ethylene glycol in a molar ratio with citric acid of 1:1. This dissolution was heated to 85 °C. The diamine–silver solution was added to the cationic solution. Subsequently, the citric acid–ethylene glycol dissolution was also added. The pH of this final mixture was adjusted to 4 with additional NH_4OH, while the temperature was increased gradually (at a rate of 5 °C/min) up to 95 °C under constant agitation. After 4 h, a translucent polymer was obtained. Further increase in temperature (150 °C) for 2 h allowed the organic phase decomposition. Then, the resultant product was pulverized and calcinated by subsequent heating at 400, 600, and 800 °C (4 h each step) followed by a final treatment of 900 °C, 24 h.

Phase constitution analysis was determined by means of X-ray diffraction (XRD) technique with Cu-K_α radiation. Crystal structure, grain size, and chemical composition were studied by transmission electron microscopy (TEM) in a JEOL ARM 200F microscope operating at 200 kV and equipped with a detector for energy-dispersive X-ray spectroscopy (EDS) analysis. Electron energy loss spectroscopy (EELS) measurements were taken with a Gatan Tridium spectrometer fitted in the microscope. X-ray photoelectron spectroscopy (XPS) measurements were carried out in a VG Microtech Multilab ESCA 2000 coupled with a CLAM4 MCD detector with Al-K_α radiation. Magnetic properties and MCE were determined by means of a physical property measuring system equipped with a vibrating sample magnetometer module (PPMS-9T, Quantum Design). In order to quantify the MCE, we use the magnetic entropy variation $|\Delta S_M|$ (for magnetic field changes ΔH of 2.0 and 5.0 T), calculated from isothermal magnetization measurements over the temperature interval

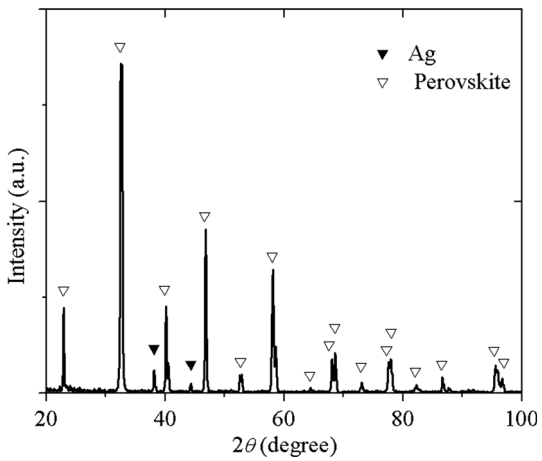

Fig. 1 XRD diffractogram for the $La_{0.80}Ag_{0.20}MnO_3$ manganite

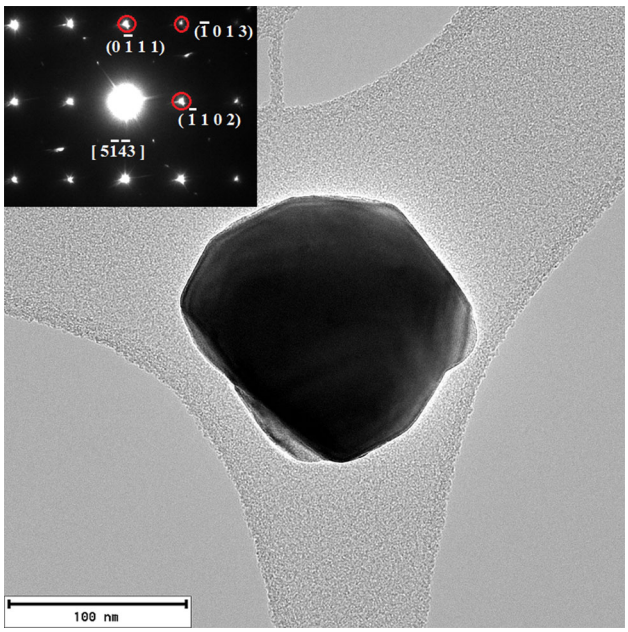

Fig. 2 Transmission electron microscopy micrograph for an isolated $La_{0.80}Ag_{0.20}MnO_3$ manganite particle. *Inset* SAED pattern showing diffracting planes from the zone axis [5 $\overline{1}$ $\overline{4}$ 3]

200–400 K, through the numerical integration of the Maxwell relation [4, 19]:

$$\Delta S_M = \int_{H_0}^{H_f} \left(\frac{\partial M}{\partial T}\right)_H dH \quad (1)$$

3 Results

XRD diffractogram for the $La_{0.80}Ag_{0.20}MnO_3$ manganite is shown in Fig. 1, for which the main phase was identified as perovskite with rhombohedral symmetry (R $\overline{3}$ c space group, ICDD-PDF 00-053-0058). Metallic silver Ag (ICDD-PDF 03-065-2871) was also observed as minor secondary phase at the peaks $2\theta = 38.1°, 44.3°$. Unlike our previous results for equivalent $La(AgSr)MnO_3$ manganites, obtained by solid-state reaction method, the Pechini synthetic route suppressed the formation of Mn_3O_4 phase, due to the calcination temperature used (of 900 °C, well below the high-temperature calcination process required for the formation of Mn_3O_4 [20]).

Transmission electron microscopy micrographs are shown in Fig. 2, for which an isolated LaAg-based manganite particle exhibits a polyhedral morphology and a size of 160 nm. Grain size variation was within the interval 150–290 nm, according to several grain micrographs (not shown). The selected area electron diffraction (SAED) pattern shown as inset in Fig. 2 corresponds to the zone axis of [5 $\overline{1}$ $\overline{4}$ 3]. Indexed planes are consistent with a rhombohedral structure (in hexagonal coordinates). Figure 3 displays an EDS mapping for a different particle, confirming chemical homogeneity, in particular, an even distribution of Ag and O atom species. Chemical

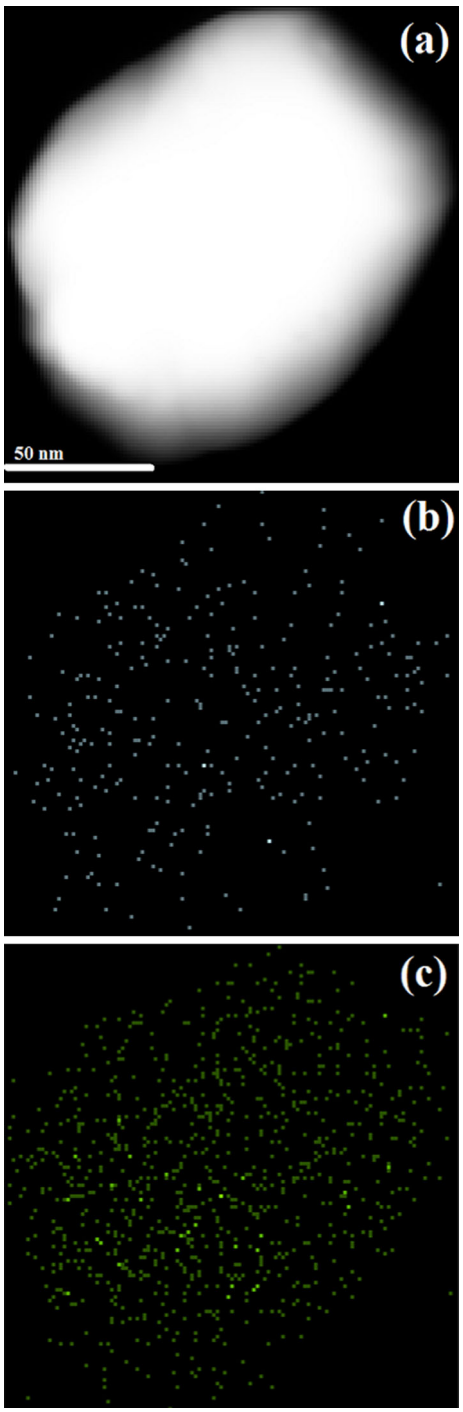

Fig. 3 EDS mapping of an isolated $La_{0.80}Ag_{0.20}MnO_3$ manganite particle, **a** selected particle, **b** Ag–L mapping, **c** O–K mapping

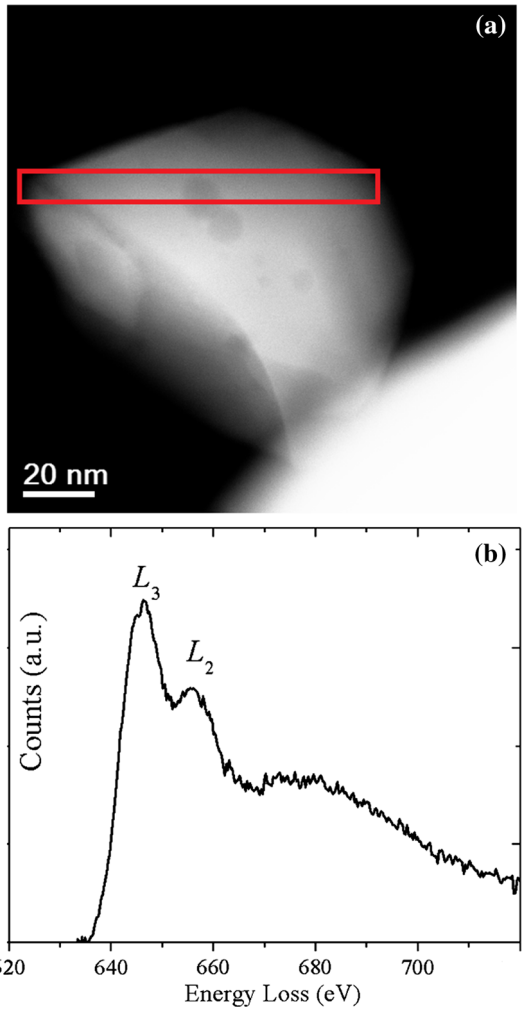

Fig. 4 **a** HAADF image for an isolated $La_{0.80}Ag_{0.20}MnO_3$ manganite particle, **b** EELS spectrum taken from the area enclosed in *red*. A preliminary background subtraction was carried by using a power law function (Color figure online)

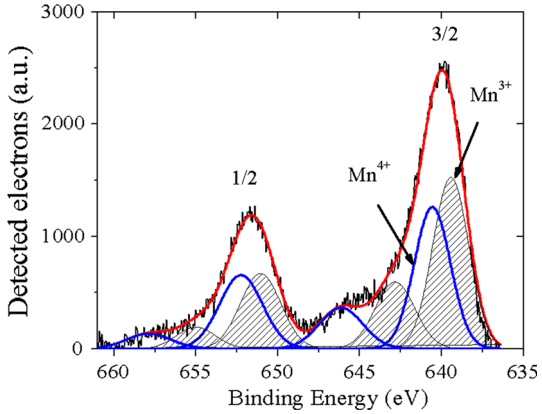

Fig. 5 High-resolution XPS spectra of the Mn2p core level for the $La_{0.80}Ag_{0.20}MnO_3$ manganite (*full line in black*). Core level energy Mn $2p_{1/2}$ corresponds to *left peak*, while *peak* on the *right* corresponds to core level Mn $2p_{3/2}$ fitting of the signal is shown as the *line in red*. Mn^{3+} peaks and satellites are shown with *shaded area*, whereas Mn^{4+} peaks and satellites are shown in *blue line* (Color figure online)

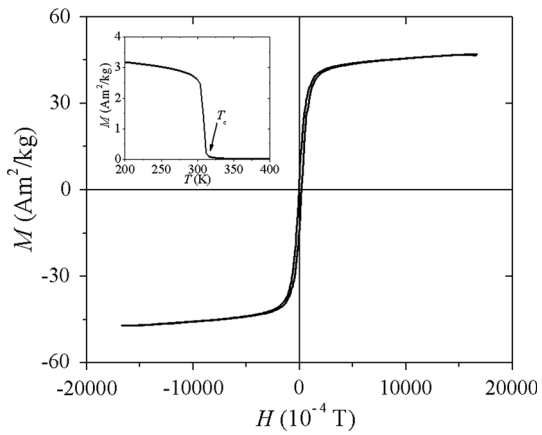

Fig. 6 Magnetization *M–H* curve for the $La_{0.80}Ag_{0.20}MnO_3$. *Inset* thermomagnetization curve showing the Curie transition

composition was quantified as an average from 10 different particles as follows: La 15.1 ± 1.9 at.%, Ag 3.4 ± 0.24 at.%, Mn 19.45 ± 4.9 at.% and O 62.05 ± 7.1 at.%, which in general, is consistent with the nominal $La_{0.80}Ag_{0.20}MnO_3$.

A critical aspect for the correlation between chemical composition and magnetic properties of La-based manganites is the mixed valence state of Mn ions, which can be Mn^{4+} or Mn^{3+} [1–4]. To quantify the mixed valence state of Mn atoms, EELS profiles were obtained on several particles in order to verify reproducibility of results. Figure 4a displays a high-angle annular dark field (HAADF) image for an isolated particle (different from Figs. 2, 3), for which an EELS spectrum (Fig. 4b) was taken from the area enclosed in red. The EELS spectrum was subtracted from background by using a power law [21]. The L_3, L_2 white-lines corresponding to the Mn-edge are visible at 646.2 and 656.1 eV, respectively. These lines appear with some overlap, due to the reduction in the energy separation between L_3, L_2 caused by the formation of Mn^{4+} ions, which contributes to a higher average valence state, relative to the Mn^{3+} state of the undoped $LaMnO_3$ phase [21]. According to the methodology proposed in [21–23], the L_3/L_2 white line intensity ratio is indicative of the average oxidation state of Mn cations. For present EELS data, after a subsequent background subtraction using an arctangent function, we obtain $L_3/L_2 = 2.25$, corresponding to a valence state between 3.4 and 3.6 [21–23]. This result reflects the presence of both Mn^{3+} and Mn^{4+} cations within the perovskite crystal structure.

In order to corroborate the mixed valence states of Mn cations in our $La_{0.80}Ag_{0.20}MnO_3$ manganite sample, XPS high-resolution spectra of the core level energies Mn $2p_{1/2}$ and Mn $2p_{3/2}$ are shown in Fig. 5. These core level signals

were used to calculate the Mn^{4+}–Mn^{3+} content by means of a deconvolution process using the peaks located at the following binding energies (BE): (a) For the Mn $2p_{3/2}$ core level, the peak at BE = 639.4 eV and its satellite at 642.9 eV (shown with shaded area) correspond to Mn^{3+}, while for Mn^{4+}, we assign the peak at 640.6 eV and its satellite at 646.2 eV (shown in blue line). (b) For the Mn $2p_{1/2}$ core level, the peak at 651.1 eV and its satellite at 654.9 eV (shaded area) correspond to Mn^{3+}, while peak at 652.2 eV and its satellite at 657.9 eV (blue line) correspond to Mn^{4+}. This assignment of peaks and satellites for Mn^{3+} and Mn^{4+} cations was proposed in [24] based on Mn $2p_{1/2}$ and Mn $2p_{3/2}$ core levels for the same LaAg-containing manganites. Mn^{3+} and Mn^{4+} contents were determined as 11.3 and 9.7 at.%, respectively, which is congruent with the total Mn content determined by EDS measurements. On the basis of this proportion, the average Mn valence is calculated as 3.4.

The magnetization curve *M–H* measured at room temperature for the $La_{0.80}Ag_{0.20}MnO_3$ is shown in Fig. 6. A strong ferromagnetic behavior with a high saturation magnetization M_s of 47 Am^2/kg is manifested, together with a sharp magnetic order–disorder transition at 308 K, associated with the Curie temperature T_c, as exhibited by the thermomagnetization *M* (*T*) curve included as inset. This ferromagnetic response represents a significant magnetic enhancement relative to the paramagnetic behavior observed for the same $La_{0.80}Ag_{0.20}MnO_3$ manganite obtained by solid-state reaction method [15]. In addition, the steep magnetic transition at T_c confirms a good chemical homogeneity, as previously indicated by EDS mapping (Fig. 3). The effect of the silver secondary phase on the manganite magnetic response is null, due to the diamagnetic character of Ag atoms.

Isothermal magnetization curves (from $H = 0$ to $H = 5.0$ T) at variable temperature for the $La_{0.80}Ag_{0.20}MnO_3$ manganite are displayed in Fig. 7a. The transition from ferromagnetic ordering to paramagnetic response (linear *M–H* curve) is visible for decreasing temperature. Arrott plots M^2 versus *H*/*M* for the same compositions are shown in Fig. 7b. The positive slope observed for these plots is indicative of a ferromagnetic–paramagnetic transition of second-order character [25].

The magnetic entropy variations $|\Delta S_m|$ as a function of temperature, calculated for $\Delta H = 2.0$ and 5.0 T according to Eq. (1) and data from Fig. 7 are displayed in Fig. 8a for the $La_{0.80}Ag_{0.20}MnO_3$ manganite. An interesting peak value of 3.2 J/kg K was recorded for $\Delta H = 2.0$, together with an excellent maximum of 5.6 J/kg K for $\Delta H = 5.0$ T.

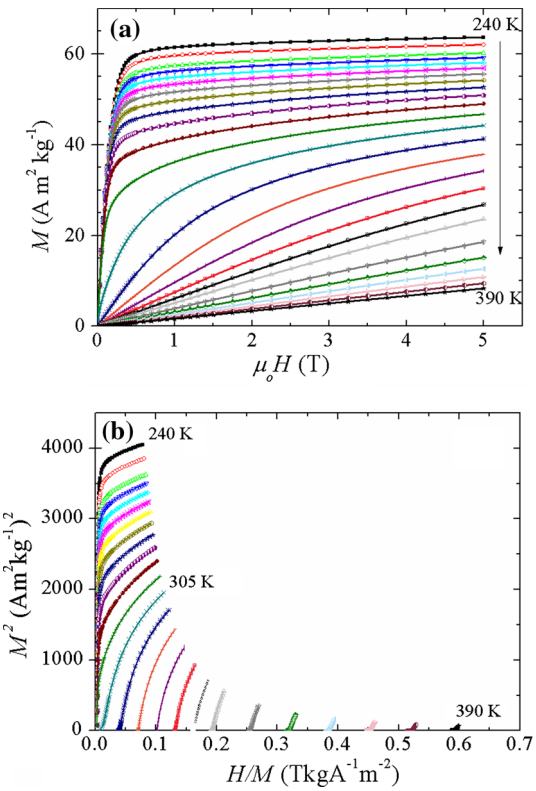

Fig. 7 **a** Isothermal magnetization curves for the $La_{0.80}Ag_{0.20}MnO_3$ manganite. **b** Arrot plots for the same sample

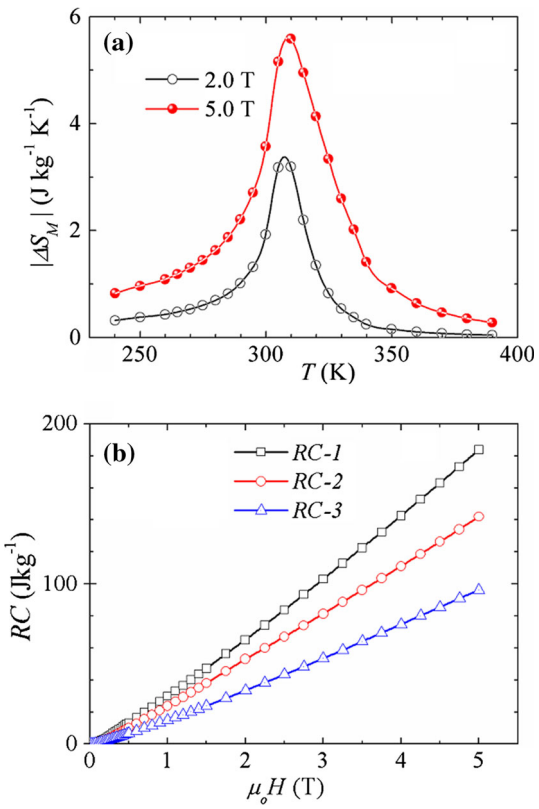

Fig. 8 **a** Magnetic entropy variations $|\Delta S_m|$ as a function of temperature for the $La_{0.80}Ag_{0.20}MnO_3$ manganite. **b** Refrigerant capacities for the same sample

These $|\Delta S_m|$ values compare very favorably with other results obtained for same $La_{0.80}Ag_{0.20}MnO_3$ manganites, for which entropy variations of 2.4 J/kg K [12], 3.2 J/kg K [14], and 2.3 J/kg K [15] have been reported. The magnetic entropy of 5.6 J/kg K results also comparable with the value reported for pure Gd (of 5.7 J/kg K at $\Delta H = 2.0$ T [26]). In addition, excellent intervals of temperature at the full-width at half maximum of the $|\Delta S_m|$ (T) curve (denoted as δT_{FWHM}) of 20 and 33 K are observed for $\Delta H = 2.0$ and 5.0 T, respectively. This δT_{FWHM} parameter is important for establishing wide thermodynamic cycles for the magnetic cooling process. Complementary, the refrigerant capacity (RC) calculated as a) RC1 = $|\Delta S_m| \times \delta T_{FWHM}$ b)RC2 = $\int |\Delta S_m| dT$ between T_{hot} and T_{cold} temperatures and c) RC3 = maximum $|\Delta S_m| \times \Delta T$ product under the $|\Delta S_m|$ (T) curve, is shown in Fig. 8b as a function of ΔH. A maximum RC-1 of 184 J/kg was observed for $\Delta H = 5.0$ T. This maximum for RC-1 is also comparable with the RC of pure Gd (of 240 J/kg for $\Delta H = 2.0$ T [1]).

4 Discussion

The mixed valence state of the Mn cations within our LaAg-based manganite is confirmed by EELS and XPS techniques, reflecting the incorporation of monovalent Ag^+ cations into the manganite crystal structure. A quantitative way to describe the stability of a perovskite structure ABO_3 (where A represents the A-sites occupied by trivalent ions and B corresponds to B-sites occupied by transition metal ions) after the incorporation of cations with variable ionic radius, is the tolerance factor t proposed by Goldschmidt [3, 27], which represents the capacity of the crystalline structure to accept additional ions at A or B-sites allowing dodecahedral and octahedral coordination, respectively. Stable crystal structures have representative t values as follows: For the ideal cubic perovskite $t = 1.0$. For the interval $0.9 < t < 1.0$, the unit cell presents a rhombohedral distortion, whereas for $t < 0.9$, the structure becomes orthorhombic [27]. The associated expression to quantify t has the following form [3, 27]:

$$(r_A + r_O) = t \cdot \sqrt{2}(r_B + r_O) \quad (2)$$

where r_A and r_B stand for the ionic radii of the A and B ions, respectively, while r_O corresponds to the ionic radii of oxygen atoms. For the present case, we should consider size, oxidation states, and relative content of the cations involved. Thus, for the following data $r_{La^{3+}} = 1.50$ Å, $r_{Ag^+} = 1.42$ Å, $r_{Mn^{3+}} = 0.72$ Å, $r_{Mn^{4+}} = 0.67$ a Å, and $r_{O^{2-}} = 1.26$ Å [28], and considering A-site occupancy for the monovalent Ag^+ ions, we use $r_A = 1.48$ Å and $r_B = 0.69$ Å to obtain $t = 0.991$, which confirms the rhombohedral deformation of the perovskite structure observed by XRD. This t value is clearly higher than the one obtained for the $La_{0.80}Ag_{0.20}MnO_3$ manganite ($t = 0.947$) synthesized by solid-state reaction route [15], which contributes to the enhanced ferromagnetic observed in this work as follows: A high tolerance factor is indicative of a more cubic-like perovskite structure favoring Mn–O–Mn angles closer to 180°, and thus, promoting the enhancement of the ferromagnetic behavior via an improved double-exchange interaction [5–7].

Silver content determined for present $La_{0.80}Ag_{0.20}MnO_3$ manganite was higher than the one observed for the sample obtained by solid-state reaction (of 2.4 at.% [15]). Higher Ag content promotes a larger number of Mn^{3+}–Mn^{4+} pairs. The importance of having a significant amount of Mn^{3+}–Mn^{4+} pairs in our LaAg-based manganite is related to the characteristic ferromagnetic coupling between them, which leads to the enhancement of the macroscopic magnetic properties M_s and T_c, and hence, to improved MCE performance. Ferromagnetic ordering between mixed valence Mn cations occurs via double-exchange (DE) interaction, a coupling mechanism first proposed by Zener [29] to explain the progressive evolution of an initial insulating antiferromagnetic $LaMnO_3$ phase (containing only Mn^{3+} cations) to a metallic ferromagnetic $(LaCa)MnO_3$ compound (containing additional Mn^{4+} ions). The partial replacement of La^{3+} for Ca^{2+} produces Mn^{4+} cations to preserve charge neutrality. The exchange interaction between Mn^{3+} and Mn^{4+} cations is through an oxygen ion, with simultaneous transfer of an electron from the Mn^{3+} (with configuration $t_{2g}^3 e_g^1$) to the oxygen, and from this to the neighboring Mn^{4+} (with configuration $t_{2g}^3 e_g^0$). This ferromagnetic Mn^{3+}–Mn^{4+} DE interaction is favored when the atoms of the transition metal are fairly separated and conduction electrons are present [29].

A complementary aspect influencing the improvement in the magnetic response is the grain size refinement attained by the Pechini synthetic route, relative to the average grain size (of 3.25 ± 0.90 μm) observed for the same $La_{0.80}Ag_{0.20}MnO_3$ manganite obtained by conventional solid-state reaction method [30]. A finer grain size distribution promotes better reactivity, together with a more homogenous oxygen distribution and hence, a more homogenous chemical composition. This chemical homogeneity has been confirmed for our LaAg-based manganite directly by EDS mapping of Fig. 3, and implicitly by the sharp Curie transition of Fig. 6. The improved ferromagnetic response attained for the $La_{0.80}Ag_{0.20}MnO_3$ manganite has a direct beneficial effect on its MCE performance, in terms of the high magnetization saturation as well as the abrupt Curie transition observed for the $M(T)$ curve, since, according to Eq. (1), $|\Delta S_M|$ is dependent on dM/dT, i.e., the slope of the $M(T)$ plot, which presents a

very well defined step at T_c and hence, favoring excellent $|\Delta S_M|$ variation within the range 3.2–5.6 J/kg K.

5 Conclusion

LaAg-based manganite synthesized by Pechini method exhibited mixed valence Mn^{3+}–Mn^{4+} states and a rhombohedral deformation of the perovskite crystal structure, due to the incorporation of Ag^{+} cations into the unit cell. The formation of Mn^{3+}–Mn^{4+} pairs promotes a noticeable enhancement of the ferromagnetic response, via double-exchange mechanism, yielding to excellent magnetocaloric performance with magnetic entropy variations as high as 5.6 J/kg K for $\Delta H = 5.0$ T, rendering this material as an interesting candidate for magnetic refrigeration applications.

Acknowledgments I. Betancourt acknowledges financial support from PASPA-UNAM, Mexico, and CONACYT Mexico, for his sabbatical leave. Electron transmission microscopy work at UTSA was supported by the NIH RCMI Nanotechnology and Human Health Core (G12MD007591). Support received from Laboratorio Nacional de Investigaciones en Nanociencias y Nanotecnología (LINAN, IPICYT) is kindly acknowledged. The valuable technical assistance by L. Huerta-Arcos, from IIM-UNAM, Mexico, is also recognized.

References

1. Franco V, Blazquez JS, Ingale B, Conde A (2012) The magnetocaloric effect and magnetic refrigeration near room temperature: materials and models. Annu Rev Mater Res 42:305–342
2. Phan Manh-Huong, Seong-Cho Yu (2007) Review of the magnetocaloric effect in manganite materials. J Magn Magn Mater 308:325–340
3. Coey JMD, Viret V, Von Molnar S (1999) Mixed-valence manganites. Adv Phys 48:167–293
4. Tishin AM, Spichkin YE (2003) The magnetocaloric effect and its applications. Institute of Physics, Bristol-Philadelphia
5. Liu SP, Tang GD, Li ZZ, Ji DH, Li YF, Chen W, Hou DL (2011) Structural and magnetic properties in the self-doped perovskite manganites with nominal composition $La_{0.7}Sr_{0.3-x}MnO_{3-\delta}$. Phys B 406:869–876
6. Bejar M, Dhahri R, El Halouani F, Dhahri E (2006) Magnetocaloric effect at room temperature in powder of $La_{0.5}(CaSr)_{0.5}MnO_3$. J Alloys Compd 414:31–35
7. Liu SP, Tang GD, Li ZZ, Qi WH, Ji DH, Li YF, Chen W, Hou DL (2011) Study of the structure, magnetic properties and free energy of the three phase composites $La_{0.7-y-z}Sr_{0.3-x}Mn_{1-\delta/3}O_{3-\delta}/(La_2O_3)_{y/2}/(La(OH)_3)_z$. J Alloys Compd 509:2320–2325
8. Aliev AM, Gamzatov AG, Batdalov AB, Mankevich AS, Korkasov IE (2011) Structure and magnetocaloric properties of $La_{1-x}K_xMnO_3$ manganites. Phys B 406:885–889
9. Tovstolytkin AI, Tsmots VM, Pankiv LI (2010) Magnetic and magnetoresistive properties of sodium-substituted lanthanum manganites. Low Temp Phys 36:220–2225
10. Koubaa M, Regaieg Y, Cheikhrouhou Koubaa W, Cheikhrouhou A, Ammar-Merah S, Herbst F (2011) Magnetic and magnetocaloric properties of lanthanum manganites with monovalent elements doping at A-site. J Magn Magn Mater 323:252–257
11. Bellakki MB, Shivakumara C, Vasanthacharya NY, Prakash AS (2010) Rapid synthesis of room temperature ferromagnetic Ag-doped $LaMnO_3$ perovskite phases by the solution combustion method. Mater Res Bull 45:1685–1691
12. The Hien N, Phu Thuy N (2002) Preparation and magneto-caloric effect of $La_{1-x}Ag_xMnO_3$ ($x = 0.10 - 0.30$) perovskite compounds. Phys B 319:168–173
13. Irmak AE, Coskun A, Tasarkuyu E, Akturk S, Unlu G, Samancioglu Y, Sarikurkcu C, Kaynar BM, Yucel A (2010) The influence of the sintering temperature on the structural and the magnetic properties of doped manganites: $La_{0.95}Ag_{0.05}MnO_3$ and $La_{0.75}Ag_{0.25}MnO_3$. J Magn Magn Mater 322:945–951
14. Tang T, Gu KM, Cao QQ, Wang DH, Zhang SY, Du YW (2000) Magnetocaloric properties of Ag-substituted perovskite-type manganites. J Magn Magn Mater 222:110–114
15. Amano ME, Betancourt I, Sánchez-Llamazares JL, Huerta L, Sánchez-Valdés CF (2014) Mixed-valence $La_{0.80}(Ag_{1-x}Sr_x)_{0.20}MnO_3$ manganites with magnetocaloric effect. J Mater Sci 49:633–641
16. Pechini MP, July 11 1967 U.S. Patent No. 3330697
17. Galceran M, Pujol MC, Aguilo M, Diaz F (2007) Sol-gel modified Pechini method for obtaining nanocrystalline KRE $(WO_4)_2$(RE = Gd and Yb). J Sol-Gel Sci Technol 42:79–88
18. Mariappan CR, Galven C, Crosnier-Lopez MP, Le Berre F, Bohnke O (2006) Synthesis of nanostructured $LiTi_2(PO_4)_3$ powder by a Pechini-type polymerizable complex method. J Solid State Chem 179:450–456
19. Brück E, Tegus O, Li XW, de Boer FR, Buschow KHJ (2003) Magnetic refrigeration: towards room-temperature applications. Phys B 327:431
20. Jacob KT, Kumar A, Rajitha G, Waseda Y (2011) Thermodynamic data for Mn_3O_4, Mn_2O_3 and MnO_2. High Temp Mater Process 30:459–472
21. Loomer DB, Al TA, Weaver L, Cogswell S (2007) Manganese valence imaging in Mn minerals at the nanoscale using STEM-EELS. Am Mineral 92:72–79
22. Shih SJ, Sharghi-Moshtaghin R, De Guire MR, Goettler R, Xing Z, Liu Z, Heuer AH (2011) Mn valence determination for lanthanum strontium manganite solid oxide fuel cell cathodes. J Electrochem Soc 158:B1276–B1280
23. Varela M, Oxley MP, Luo W, Tao J, Watanabe M, Lupini AR, Pantelides ST, Pennycook SJ (2009) Atomic-resolution imaging of oxidation states in manganites. Phys Rev B 79:085117
24. Kucharczyk B, Tylus W (2008) Partial substitution of lanthanum with silver in the LaMnO3 perovskite: effect of the modification on the activity on monolithic catalysts in the reactions of methane and carbon oxide oxidation. Appl Catal A Gen 335:28–36
25. Banerjee BK (1964) On a generalized approach to first and second order magnetic transitions. Phys Lett 12:16–17
26. Dankov SY, Tishin AM, Pecharsky VK, Gschneidner KA (1998) Magnetic phase transitions and the magnetothermal properties of gadolinium. Phys Rev B 57:3478–3490
27. Attfield JP (1998) A simple approach to lattice effects in conducting perovskite-type oxides. Chem Mater 10:3239–3248
28. Shannon RD (1976) Revised effective ionic radii and systematic studies of interatomic distances in halides and chalcogenides. Acta Crystallogr A 32:751–761
29. Zener C (1951) Interaction between the d shells in the transition metals. Phys Rev B 81:440–445
30. Amano Patiño ME (2011) Synthesis, structure and magnetic properties of La(Ag, Sr)MnO3 manganites. Faculty of Chemistry, National Autonomoues University of Mexico, Thesis